

(A New Proposal to Jefferson Lab PAC-30)

Measurement of Neutron Spin Asymmetry A_1^n in the Valence Quark Region
Using an 11 GeV Beam and a Polarized ^3He Target in Hall C

July 9, 2006

S. Zhou, X. Li

China Institute of Atomic Energy, Beijing 102413, P.R. China

H. Gao, X. Qian, X.F. Zhu

Duke University, Durham, NC 27708

P. Markowitz

Florida International University, Miami, FL 33199

C. Keppel, E. Christy, V. Tvaskis

Hampton University, Hampton, VA 23668

A. Bruell, A. Camsonne, J.-P. Chen (co-spokesperson), E. Chudakov, A. Deur, R. Ent
O.-J. Hansen, D. W. Higinbotham, T. Horn, M. Jones, D. Mack, A. Saha

Jefferson Lab, Newport News, VA 23606

A.T. Katramatou, E. Khrosinkova, G.G. Petratos

Kent State University, Kent, OH 44242

K. Allada, C. Dutta, A. Kolarkar, W. Korsch

University of Kentucky, Lexington, KY 40506

K. Kumar, K. Paschke ¹

University of Massachusetts at Amherst, Amherst, MA 01003

W. Bertozzi, S. Gilad, X. Zheng (co-spokesperson) ²

Massachusetts Institute of Technology, Cambridge, MA 02139

J. Dunne, D. Dutta

Mississippi State University, Mississippi State, MS 39762

R. Gilman

Rutgers, The State University of New Jersey, Piscataway, NJ 08855

H. Lu, X. Yan, Y. Ye

University of Science and Technology of China, Hefei, Anhui 230026, P.R. China

¹Affiliation starting September 2006: University of Virginia, Charlottesville, VA 22904

²contact person, email: xiaochao@jlab.org. Affiliation starting September 2006: University of Virginia, Charlottesville, VA 22904

Seonho Choi, Hyekoo Kang, Byungwuek Lee, Yumin Oh, Jongsog Song
Seoul National University, Seoul 151-747, Korea

P. Souder
Syracuse University, Syracuse, NY 13244

Z. E. Meziani (co-spokesperson), B. Sawatzky
Temple University, Philadelphia, PA 19122

G. D. Cates (co-spokesperson), D. Crabb, D. Day, N. Liyanage, O.A. Rondon, K. Slifer
University of Virginia, Charlottesville, VA 22904

D. Armstrong, T. Averett, M. Finn, K. Grimm, T. Holmstrom, A. Kelleher, V. Sulkosky
College of William and Mary, Williamsburg, VA 23187

S. Sirca
University of Ljubljana, Slovenia

Abstract

We propose here precision measurements of the neutron spin asymmetry A_1^n in the deep inelastic scattering region $0.3 < x < 0.77$ and $3 < Q^2 < 10$ (GeV/c)². We plan to use a polarized ³He target in Hall C, together with the high momentum spectrometer (HMS) and the planned Super HMS (SHMS). The wide Q^2 span of this measurement will explore possible Q^2 -dependence of A_1^n . The proposed measurement will provide the first precision data in the valence quark region above $x = 0.6$ and therefore test various predictions including those from the relativistic constituent quark model and perturbative QCD.

The polarized ³He group will install the polarized ³He target in Hall C. In addition, the University of Virginia group (lead by spokespersons Gordon Cates and Xiaochao Zheng) and the Temple University group (lead by spokesperson Zein-Eddine Meziani) are committed to make at least 2 FTE-years contribution to Hall C beamline commissioning at the 12 GeV Upgrade, including the Compton and the Moller polarimeters, the ARC energy measurement and the fast raster system.

In this document, we first review physics motivation of the A_1^n measurement. We then present the experimental setup, including the polarized ³He target we plan to install in Hall C. Next we give rate estimation and projected results, and summarize the beam time request in the end.

Contents

1	Physics Motivation	4
1.1	Nucleon Spin Valence (Large x) Structure	4
1.2	Theoretical Predictions for A_1 at Large x_{Bj}	5
1.2.1	SU(6) Non-Relativistic Constituent Quark Model	5
1.2.2	SU(6) Breaking and Hyperfine Perturbed Relativistic CQM	6
1.2.3	Perturbative QCD and Hadron Helicity Conservation	7
1.2.4	Predictions from Next-to-Leading Order QCD Fits	7
1.2.5	Predictions from Chiral Soliton and Instanton Models	8
1.2.6	Other Predictions	8
1.3	Existing Data	8
1.4	About the Q^2 -Dependence of A_1	8
2	The Measurement	10
2.1	The Electron Beam	10
2.2	Spectrometers	10
2.3	The Polarized ^3He Target	10
2.4	Kinematics	13
2.5	Pion Background	13
2.6	Pair Production Background	15
2.7	Elastic and $\Delta(1232)$ Asymmetries	17
3	Data Analysis and Systematic Uncertainties	17
3.1	Data Analysis Procedure for $A^{3\text{He}}$	17
3.2	Nuclear Corrections	18
3.3	Systematic Uncertainties	18
4	Expected Results and Complementarity to the Hall A BigBite Proposal	19
4.1	Expected Results for A_1^n and Uncertainties	19
4.2	Expected Results for Neutron $h^{g1}(x)$	22
4.3	Complementarity to the Hall A proposal	22
5	Beam Time Request and Contributions to Hall C 12 GeV Equipment	24
5.1	Beam Time Request	24
5.2	Contributions to Hall C 12 GeV Equipment	25
6	Summary	25

1 Physics Motivation

1.1 Nucleon Spin Valence (Large x) Structure

Interest in the spin structure of the nucleon became prominent in the 1980's when experiments at CERN [1, 2] and SLAC [3, 4] on the integral of the proton polarized structure function g_1^p showed that the total spin carried by quarks was very small, $\approx (12 \pm 17)\%$ [1, 2]. This was in contrast to the simple relativistic valence quark model prediction [5, 6, 7, 8, 9, 10, 11, 12] in which the spin of quarks carries approximately 75% of the proton spin and the remaining 25% comes from their orbital angular momentum. Because the quark model is very successful in describing static properties of hadrons, the fact that the quark spins account for only a small part of the nucleon spin was a big surprise and generated very productive experimental and theoretical activities to the present. Current understanding [13, 14, 15] of the nucleon spin is that the total spin is distributed among valence quarks, $q\bar{q}$ sea quarks, their orbital angular momenta, and gluons. This is called the nucleon spin sum rule:

$$S_z^N = S_z^q + L_z^q + J_z^g = \frac{1}{2}, \quad (1)$$

where S_z^N is the nucleon spin, S_z^q and L_z^q represent respectively the quark spin and orbital angular momentum (OAM), and J_z^g is the total angular momentum of the gluons. Only about $(20 - 30)\%$ of the nucleon spin is carried by the spin of the quarks. To further study the nucleon spin, one thus needs to know more precisely how it decomposes into the three components in the full x and Q^2 region, and to understand data from the standard model of strong interactions – Quantum Chromodynamics (QCD). However, due to the highly non-perturbative feature of strong interactions, it is extremely difficult to make absolute predictions from QCD on the nucleon spin.

The high x region, however, may provide an exception to this difficulty: Because the $q\bar{q}$ sea and gluons are scarce in the large x region, the nucleon is viewed as made primarily of three valence quarks and its spin is carried only by the valence quarks (the large x region is also called the “valence quark region” because of this reason), and one might estimate ratios of structure functions (which can be related to the quark spin) based on our knowledge of interactions between quarks. Secondly, the constituent quark model which works very well in predicting the static properties of the nucleon, should work for valence quarks. Hence the valence quark region provides a unique place to test whether constituent quark model also works in describing the dynamic properties of the nucleon probed in deep inelastic scatterings (DIS). In this section we will review a majority of theoretical predictions and models as well as existing measurements.

Our focus here is the virtual photon asymmetry A_1 , defined as

$$A_1(x, Q^2) \equiv \frac{\sigma_{1/2} - \sigma_{3/2}}{\sigma_{1/2} + \sigma_{3/2}}$$

where $\sigma_{1/2(3/2)}$ is the nucleon's photo-absorption cross section with total helicity of the $\gamma^* - N$ system being $1/2(3/2)$. A_1 can be related to the unpolarized and the polarized structure functions F_1 and g_1 as

$$A_1(x, Q^2) = \frac{g_1(x, Q^2) - \gamma^2 g_2(x, Q^2)}{F_1(x, Q^2)} \quad (2)$$

where $\gamma^2 \equiv \frac{Q^2}{\nu^2} = \frac{(2Mx)^2}{Q^2}$ and at large Q^2 one has $A_1 \approx g_1/F_1$. The structure functions F_1 and g_1 have explicit implication in the quark-parton model:

$$F_1(x, Q^2) = \frac{1}{2} \sum_i e_i^2 q_i(x, Q^2) \quad \text{and} \quad g_1(x, Q^2) = \frac{1}{2} \sum_i e_i^2 \Delta q_i(x, Q^2), \quad (3)$$

where $q_i(x, Q^2) = q_i^\uparrow(x, Q^2) + q_i^\downarrow(x, Q^2)$ and $\Delta q_i(x, Q^2) = q_i^\uparrow(x, Q^2) - q_i^\downarrow(x, Q^2)$ are the unpolarized and the polarized parton distribution functions, respectively.

1.2 Theoretical Predictions for A_1 at Large x_{Bj}

1.2.1 SU(6) Non-Relativistic Constituent Quark Model

In the simplest non-relativistic constituent quark model (CQM) [16, 17], the nucleon is made of three constituent quarks and the nucleon spin is fully carried by the quark spin. Assuming SU(6) symmetry, the wavefunction of a neutron polarized in the $+z$ direction then has the form [5]:

$$\begin{aligned} |n \uparrow\rangle &= \frac{1}{\sqrt{2}} |d^\uparrow(du)_{000}\rangle + \frac{1}{\sqrt{18}} |d^\uparrow(du)_{110}\rangle \\ &\quad - \frac{1}{3} |d^\downarrow(du)_{111}\rangle - \frac{1}{3} |u^\uparrow(dd)_{110}\rangle + \frac{\sqrt{2}}{3} |u^\downarrow(dd)_{111}\rangle, \end{aligned} \quad (4)$$

where the two spectator quarks form a ‘‘diquark’’ state and the three subscripts are the diquark's total isospin, total spin (S) and the spin projection along the $+z$ direction (S_z). For the case of a proton one needs to exchange the u and d quarks in Eq. (4). In the limit where SU(6) symmetry is exact, both diquark spin states with $S = 1$ and $S = 0$ contribute equally to the observables of interest, leading to the predictions

$$A_1^p = 5/9, \quad A_1^n = 0, \quad \Delta u/u = 2/3, \quad \text{and} \quad \Delta d/d = -1/3. \quad (5)$$

In the case of DIS, exact SU(6) symmetry implies the same shape for the valence quark distributions, *i.e.* $u(x) = 2d(x)$. Assuming that $R(x, Q^2) \equiv \sigma_L/\sigma_T$ is the same for the neutron and the proton, one can write the ratio of neutron and proton F_2 structure functions as

$$R^{np} \equiv \frac{F_2^n}{F_2^p} = \frac{u(x) + 4d(x)}{4u(x) + d(x)}. \quad (6)$$

Applying $u(x) = 2d(x)$ gives $R^{np} = 2/3$. However, data on the R^{np} ratio from SLAC [18, 19, 20], CERN [21, 22, 23, 24, 25] and Fermilab [26] disagree with this SU(6) prediction. The data show that $R^{np}(x)$ is a straight line starting with $R^{np}|_{x \rightarrow 0} \approx 1$ and dropping to below 1/2 as $x \rightarrow 1$. In addition, $A_1^p(x)$ is small at low x [1, 2, 27, 28]. The fact that $R^{np}|_{x \rightarrow 0} \approx 1$ may be explained by the presence of a dominant amount of sea quarks in the low x region and the fact that $A_1^p|_{x \rightarrow 0} \approx 0$ could be because these sea quarks are not highly polarized. At large x , however, there are few sea quarks and the deviation from SU(6) prediction indicates a problem with the wavefunction described by Eq. (4). In fact, SU(6) symmetry is known to be broken [29, 30] and the details of possible SU(6)-breaking mechanisms is an important open issue in hadronic physics.

1.2.2 SU(6) Breaking and Hyperfine Perturbed Relativistic CQM

A possible explanation for the SU(6) symmetry breaking is the one-gluon exchange interaction which dominates the quark-quark interaction at short-distances. This interaction was used to explain the behavior of R^{np} near $x \rightarrow 1$ and the ≈ 300 -MeV mass shift between the nucleon and the $\Delta(1232)$ [29, 30]. Later this was described by an interaction term proportional to $\vec{S}_i \cdot \vec{S}_j \delta^3(\vec{r}_{ij})$, with \vec{S}_i the spin of the i^{th} quark, hence is also called the hyperfine interaction, or chromomagnetic interaction among the quarks [31]. The effect of this perturbation on the wavefunction is to lower the energy of the $S = 0$ diquark state, causing the first term of Eq. (4), $|d \uparrow (ud)_{000}\rangle$ (for the neutron), to become more stable and to dominate the high energy tail of the quark momentum distribution that is probed as $x \rightarrow 1$. Since the struck quark in this term has its spin parallel to that of the nucleon, the dominance of this term as $x \rightarrow 1$ implies $(\Delta d/d)^n \rightarrow 1$ and $(\Delta u/u)^n \rightarrow -1/3$ for the neutron, while for the proton one has

$$\Delta u/u \rightarrow 1 \text{ and } \Delta d/d \rightarrow -1/3 \text{ as } x \rightarrow 1. \quad (7)$$

One also obtains $R^{np} \rightarrow 1/4$ as $x \rightarrow 1$, which could explain the deviation of $R^{np}(x)$ data from the SU(6) prediction. Based on the same mechanism, one can make the following predictions:

$$A_1^p \rightarrow 1 \text{ and } A_1^n \rightarrow 1 \text{ as } x \rightarrow 1. \quad (8)$$

The hyperfine interaction is often used to break SU(6) symmetry in the relativistic CQM (RCQM). In this model, the constituent quarks have non-zero OAM which carries $\approx 25\%$ of the nucleon spin [5, 6, 7, 8, 9, 10, 11, 12]. The use of RCQM to predict the large x behavior of the nucleon structure functions can be justified by the valence quark dominance, *i.e.*, in the large x region almost all quantum numbers, momentum and the spin of the nucleon are carried by the three valence quarks, which can therefore be identified as constituent quarks. Predictions of A_1^n in the large x region using the hyperfine-perturbed RCQM have been achieved [32].

1.2.3 Perturbative QCD and Hadron Helicity Conservation

In the early 1970's, in one of the first applications of perturbative QCD (pQCD), it was noted that as $x \rightarrow 1$, the scattering is from a high-energy quark and thus the process can be treated perturbatively [33]. Furthermore, when the quark OAM is assumed to be zero, the conservation of angular momentum requires that a quark carrying nearly all the momentum of the nucleon (*i.e.* $x \rightarrow 1$) must have the same helicity as the nucleon. This mechanism is called hadron helicity conservation (HHC), and is sometimes referred to as the leading-order pQCD. In this picture, quark-gluon interactions cause only the $S = 1$, $S_z = 1$ diquark spin projection component rather than the full $S = 1$ diquark system to be suppressed as $x \rightarrow 1$, which gives

$$\Delta u/u \rightarrow 1 \text{ and } \Delta d/d \rightarrow 1 \text{ as } x \rightarrow 1 ; \quad (9)$$

$$R^{np} \rightarrow \frac{3}{7}, \quad A_1^p \rightarrow 1 \text{ and } A_1^n \rightarrow 1 \text{ as } x \rightarrow 1 . \quad (10)$$

This is one of the few places where pQCD can make an absolute prediction for the x -dependence of the structure functions or their ratios. However, how low in x and Q^2 this picture works is uncertain. HHC has been used as a constraint in a model to fit data on the first moment of the proton g_1^p , giving the BBS parameterization [34]. The Q^2 evolution was not included in this calculation. Later in the LSS(BBS) parameterization [35], both proton and neutron A_1 data were fitted directly and the Q^2 evolution was carefully treated. Predictions for A_1^n using both BBS and LSS(BBS) parameterizations have been made.

HHC is based on the assumption that the quark OAM is zero. However, recent experimental data on the tensor polarization in elastic $e-^2\text{H}$ scattering [36], neutral pion photo-production [37], the proton electro-magnetic form factors [38, 39], as well as the A_1^n data from JLab 6 GeV [40, 41], disagree with the HHC predictions [42]. It has been suggested that effects beyond leading-order pQCD, such as quark OAM [43, 44, 45, 46], might play an important role in processes involving quark spin flips.

1.2.4 Predictions from Next-to-Leading Order QCD Fits

In a next-to-leading order (NLO) QCD analysis of the world data [47], parameterizations of the polarized and unpolarized PDFs were performed without the HHC constraint. Predictions of g_1^p/F_1^p and g_1^n/F_1^n were made using these parameterizations.

In a statistical approach, the nucleon is viewed as a gas of massless partons (quarks, antiquarks and gluons) in equilibrium at a given temperature in a finite volume, and the parton distributions are parameterized using either Fermi-Dirac or Bose-Einstein distributions [48]. Based on this statistical picture of the nucleon, a global NLO QCD analysis of unpolarized and polarized DIS data was performed. In this calculation $\Delta u/u \approx 0.75$, $\Delta d/d \approx -0.5$ and $A_1^{p,n} < 1$ at $x \rightarrow 1$.

1.2.5 Predictions from Chiral Soliton and Instanton Models

While pQCD works well in high-energy hadronic physics, theories suitable for hadronic phenomena in the non-perturbative regime are much more difficult to construct. Possible approaches in this regime are quark models, chiral effective theories and the lattice QCD method. Predictions for $A_1^{n,p}$ have been made using chiral soliton models [49, 50, 51] and [52, 53] and the latter give $A_1^n < 0$.

1.2.6 Other Predictions

Other predictions include those from bag model [54, 55] and quark-hadron duality [56, 57]. In the duality model, one obtains the structure functions and their ratios in the large x region by summing over matrix elements for nucleon resonance transitions. To incorporate SU(6) breaking, different mechanisms consistent with duality were assumed and data on the structure function ratio R^{np} were used to fit the SU(6) mixing parameters. In this picture, $A_1^{n,p} \rightarrow 1$ as $x \rightarrow 1$ is a direct result. Duality predictions for $A_1^{n,p}$ using different SU(6) breaking mechanisms were performed in Ref. [58].

1.3 Existing Data

The DIS cross section is determined by the parton distribution functions (PDF) of the nucleon and the Mott component. Because the nucleon PDFs are low in the large x region, and because large x implies high Q^2 , which further reduce the Mott cross section, the probability for scattering to occur is extremely low at high x . Due to this experimental limitation, the large x region had not been well explored until the continuous electron beam at JLab became operational. In 2001, taking the advantage of the polarized beam and a polarized ^3He target in Hall A, we had for the first time measured the neutron spin structure above $x > 0.4$. Results from this experiment [40, 41] have shown a clear trend that A_1^n turns to positive above $x = 0.5$. However, the datum at the highest x (0.6) is still far from the RCQM and the pQCD (with HHC) predictions, although they agree pretty well with calculations from most NLO QCD parameterizations. In particular, results on polarized PDF $\Delta d/d$ extracted from these A_1^n results do not agree with the HHC prediction. It is therefore crucial to extend the A_1^n measurement to a higher x and wider Q^2 region to determine whether pQCD (with HHC) or RCQM holds.

1.4 About the Q^2 -Dependence of A_1

From Eq.(2) one can deduce that $A_1 \approx g_1/F_1$ at large Q^2 . One can then naively expect that the Q^2 -evolution of g_1 and F_1 follow the same rule in the framework of perturbative QCD and cancel exactly in their ratio, hence A_1 becomes independent of Q^2 . Unfortunately this is not true even if one ignored the obvious $\gamma^2 g_2$ term (which cannot be neglected in the kinematic region achievable at JLab): Only the leading-order and the

next-to-leading-order Q^2 -evolution of g_1 and F_1 follow the same rule, while their higher orders ($\geq N^2\text{LO}$) and higher twist contributions are different. Therefore, although there is some evidence from data that $A_1(x, Q^2)$ is almost independent of Q^2 and it has almost become a tradition in experimental practice to ignore it, there is no justification for believing A_1 to be exactly constant [59]. *Measurement of the Q^2 -dependence of $A_1(x, Q^2)$, therefore, has become important as our study of this asymmetry goes beyond the stage of mere exploration.* In particular, modern examination of our understanding of the nucleon spin often involve comparison of lattice QCD calculations with precision measurements of moments of structure functions, where for the latter data have to be accurately evolved to the same Q^2 for integrations.

Typically, one can write for $g_1(x, Q^2)$ [60]:

$$g_1(x, Q^2) = g_1(x, Q^2)_{LT} + g_1(x, Q^2)_{HT} \quad (11)$$

where ‘‘LT’’ denotes the leading twist ($\tau = 2$) contribution to g_1 , while ‘‘HT’’ denotes contributions to g_1 arising from QCD operators of higher twist, namely $\tau \geq 3$. The LT contribution can be further written as

$$g_1(x, Q^2)_{LT} = g_1(x, Q^2)_{pQCD} + h^{TMC}(x, Q^2)/Q^2 + \mathcal{O}(M^4/Q^4) \quad (12)$$

where $g_1(x, Q^2)_{pQCD}$ is the well known (logarithmic in Q^2) pQCD contribution and $h^{TMC}(x, Q^2)$ are the calculable kinematic target mass corrections, which effectively could belong to the LT term. The HT contribution can be written as

$$g_1(x, Q^2)_{HT} = h(x, Q^2)/Q^2 + \mathcal{O}(\Lambda^4/Q^4) \quad (13)$$

where $h(x, Q^2)$ are the dynamical higher twist ($\tau = 3$ and $\tau = 4$) corrections to g_1 . The dynamical HT are related to multi-parton correlations in the nucleon, are non-perturbative and cannot be calculated without using models. Similar descriptions as Eq.(11-13) also work for $F_1(x, Q^2)$. Among all contributions, only the LO and NLO terms of $g_1(x, Q^2)_{pQCD}$ and $F_1(x, Q^2)_{pQCD}$ have the same Q^2 -dependences.

In Ref. [60] a formalism was presented to extract the higher-twist contribution to g_1 from data:

$$\left[\frac{g_1(x, Q^2)}{F_1(x, Q^2)} \right]_{exp} = \frac{g_1(x, Q^2)_{LT} + h(x)/Q^2}{F_1(x, Q^2)_{exp}}. \quad (14)$$

where $F_1(x, Q^2)$ is replaced by its expression in terms of the usually extracted from unpolarized DIS experiments F_2 and R . Eq. (14) provides a model-independent way to extract the HT term from data. Results for $h^{g_1}(x)$ for the proton and the neutron were presented in. However h^{n, g_1} is found to be consistent with zero above $x = 0.2$.

2 The Measurement

We propose to measure inclusive deep inelastic scattering of longitudinally polarized electrons from a polarized ^3He target in Hall C. To precisely extract A_1 the target spin needs to be aligned both parallel and perpendicular to the beamline. To check the product of beam and target polarizations $P_b P_t$ and other systematics, we will measure the longitudinal asymmetry of $\vec{e} - ^3\vec{\text{He}}$ elastic scattering and the transverse asymmetry of $\Delta(1232)$ production at low Q^2 . We will also take some DIS data with spectrometers in a reversed polarity mode to check the pair production background and its asymmetry.

2.1 The Electron Beam

We plan to use 11 GeV electron beam for the proposed DIS measurement and 2.2 GeV for elastic and $\Delta(1232)$ asymmetry measurements. The beam charge asymmetry needs to be controlled below 200 ppm throughout the measurement.

Both the current Moller and the planned Compton polarimeters in Hall C will be used to measure the beam polarization. Both polarimetry are expected to provide a precision of $\Delta P_b/P_b < 1\%$ with some effort. The regular beam charge and beam position monitors will be used to ensure the beam quality and provide measurement of the beam charge asymmetry for data analysis. To limit the heat and radiation impact on the target glass cells, the beam rastering system will be used such that the beam spot on target has a circular shape and is 5 mm in diameter.

2.2 Spectrometers

To reach high x it is necessary to use the highest beam energy available and detect the scattered electrons at a relatively large angle. We will use both the HMS and the SHMS at similar kinematic settings to collect data. Figure 1 shows a schematic top view of the hall with these two spectrometers in position. The basic angle and momentum ranges and acceptances of HMS and SHMS are listed in table 1. To reject the typical high pion background in DIS region a atmospheric gas Čerenkov and a multiple-layer lead-glass shower counter need to be used. These detectors already exist for the HMS, and for the SHMS they are being designed as part of the basic detector package [61]. The expected pion rejection efficiency is greater than 1×10^4 .

2.3 The Polarized ^3He Target

The polarized ^3He target at JLab is based on optical pumping of a vapor of alkali atoms and subsequent spin exchange between the polarized atoms and the ^3He nuclei.

Figure 2 shows the basic layout of the polarized ^3He target which currently exists for research in Hall A [62]. The target holding field is provided by two sets of Helmholtz coils oriented normal to each other, hence the target spin direction can be aligned either

Figure 1: Schematic view of Hall C with the HMS and the SHMS

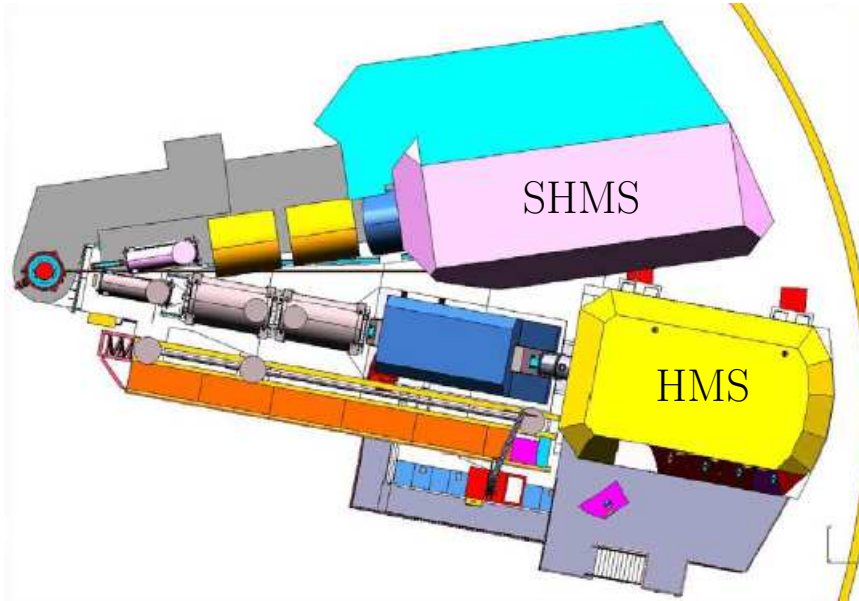


Table 1: Angle and momentum ranges and acceptances of HMS and SHMS.

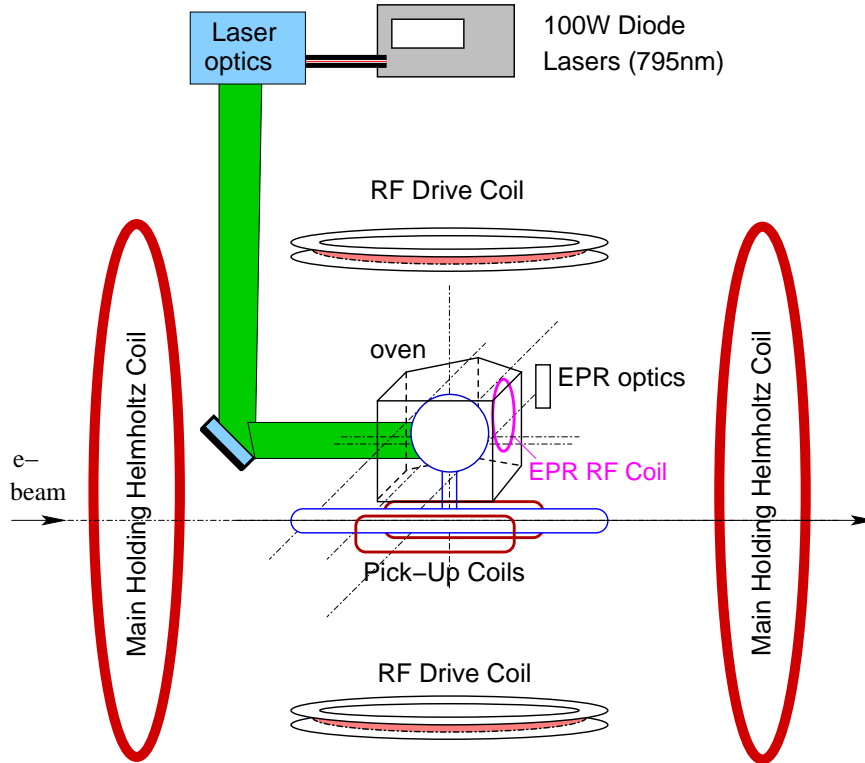
Spectrometer	p range (GeV/ c)	θ range	$\Delta p/p$	solid angle (msr)	y_{targ} (cm)
HMS	0.5-7.5	$12.5^\circ - 90^\circ$	(-9.0%, +9.0%)	8.0	10
SHMS	2.0-10.4	$5.5^\circ - 30^\circ$	(-15.0%, 25.0%)	3.8	30

parallel or perpendicular to the electron beam. Fig. 3 shows a picture of a standard 40 cm long cell. The cells for these experiments consist of a two chamber design. The upper spherical chamber contains the alkali vapor while the lower chamber is used for electron scattering from the polarized ^3He .

Approximately 100 Watts (total) of light from a set of 3-4 diode lasers is combined using an optical fiber coupler and directed through a series of optics to produce circularly polarized light at a wavelength of ~ 795 nm. This light is used to polarize the alkali vapor through optical pumping. The polarized alkali transfers its spin to the ^3He nuclei through collisions.

This target has been used by seven experiments in Hall A from 1998 to 2006 and is currently being re-designed for a series of five experiments planned for 2007 as shown in Figure 4. In addition to adding a third set of Helmholtz coils to allow for polarization in the vertical direction, the new system will incorporate new design features allowing it to capitalize on the recent success of a similar target used for experiment E02-013 [63]. So-called ‘hybrid’ target cells [64] containing a mixture of potassium and rubidium were

Figure 2: Typical layout of a polarized ^3He target. Note that for simplicity, only one of the three sets of orthogonal Helmholtz coils shown.

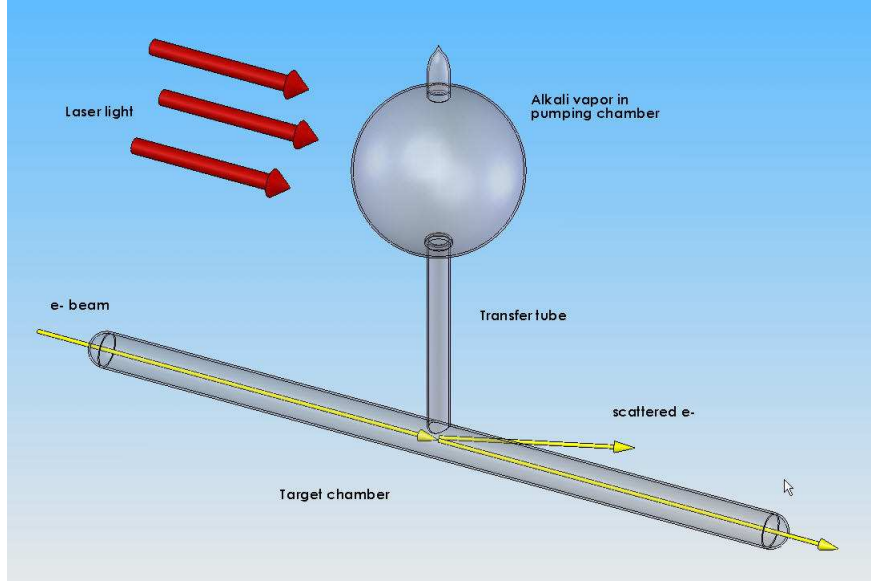


used to achieve about 55% polarization with $8 \mu\text{A}$ of beam current. During E02-013 a single cell was used with a beam current of $8 \mu\text{A}$ for 6 weeks without rupturing. Beam currents up to $15 \mu\text{A}$ could be used with a degradation in polarization and cell lifetime.

The target polarization can be measured using two methods: NMR and EPR (Electron-Paramagnetic Resonance). Each type of polarimetry can provide a relative 4% precision and the result from the two combined will have a 3% precision. In this document we use a polarization of $50\%(1 \pm 3\%)$ to estimate the expected uncertainties and beam time request. With a maximum beam current of $15 \mu\text{A}$ and a typical target density of 12 amg under operating conditions, this provides a $e - \vec{n}$ luminosity of $1 \times 10^{36} \text{ s}^{-1} \text{ cm}^{-2}$ [62].

This target continues to be a flagship facility for the Hall A program and will be relatively easy to adapt for use at 11 GeV in Halls A and C. Polarized target groups at the College of William and Mary and the University of Virginia continue to produce target cells with consistently-improving polarization. Through the combined effort of these groups and the polarized target groups and personnel at the University of Kentucky, Temple University, Duke University and Jefferson Lab this collaboration has the necessary experience and manpower for this polarized target system.

Figure 3: A standard polarized ^3He target cell. The cell consists of a spherical “pumping chamber,” a cylindrical “target chamber,” and a “transfer tube” connecting the two chambers. The electron beam passes through the 40 cm long target chamber as shown.



Under typical running conditions, heat from the pumping lasers and radiation from the beam will deteriorate the target cell quickly, causing the cell glass wall to be less transparent. To avoid glass rupture due to excessive heat absorption in the glass, the cell needs to be replaced at least every month. For a 2-month long experiment as proposed here, at least four cells will be needed (three for production and at least one for spare).

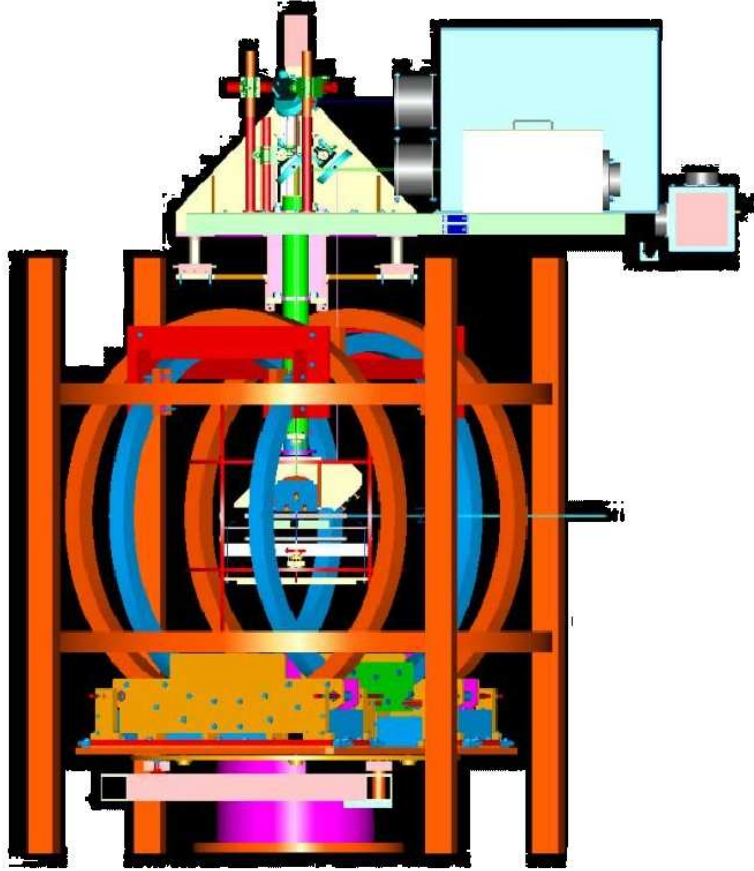
2.4 Kinematics

The kinematics used and estimated beam time are given in table 2. The HMS has 4 settings (1,2,3,4) and the SHMS has 3 settings (A,B,C). The SHMS setting A(C) has the same x and Q^2 coverages as HMS settings 1 and 2 (4 and 5), and covers the large (small) x regions. The SHMS setting B is used to cover the low x but high Q^2 region in order to explore the Q^2 -dependence of A_1^n within $0.35 < x < 0.55$. The Q^2 and x coverages of the measurement are shown in Fig. 8. The wide Q^2 -span at medium x bins helps to explore possible Q^2 -dependence of A_1^n .

2.5 Pion Background

The dominant background of DIS inclusive measurement is usually the pion production process. During past experiments the asymmetry of pion productions of doubly-polarized

Figure 4: Current design (side view) of the Hall A polarized target system for the series of experiments planned for 2007-08. It is expected that this target system can be used with little modification for the 11 GeV programs in Halls A and C. Though the target itself is well-suited for use in Hall A or C, a new mounting system at the pivot, and accommodations for the lasers, will be needed for use in Hall C.



scattering was observed to be large, typically 10 times higher than DIS electron asymmetry. We require that the relative uncertainty on our measurement asymmetry due to pion background to be less than 4%, then the pion rejection factor, $\eta_{\pi, rej}$, needs to be at least $\alpha_{\pi/e} \times 10 / (4\%)$, with $\alpha_{\pi/e}$ the π/e ratio. This requires the combined pion rejection factor of a gas Čerenkov and a lead-glass shower counter to be at least 10^3 . From our past experience this can be achieved without much difficulty from careful off-line calibrations and particle identification (PID) analysis.

In addition, the asymmetry of pion background can be measured simultaneously with

Table 2: Kinematics for large x measurements of the A_1^n asymmetries at JLab 12 GeV Upgrade in Hall C. Both HMS and SHMS will be used at similar settings. The π and e^+ background rates are conservative estimations using the Wiser's fit [65].

	Kine	E_b GeV	E_p GeV	θ ($^\circ$)	DIS (e, e') rate (Hz)	π^-/e	e^+/e^-	x (Q^2 , in GeV 2) coverages for DIS
1	HMS	11.0	5.70	12.5	498.17	< 0.5	$< 0.1\%$	0.25-0.35 (2.78- 3.17)
2	HMS	11.0	6.80	12.5	370.41	< 0.1	$< 0.1\%$	0.35-0.55 (3.26- 3.78)
3	HMS	11.0	2.82	30.0	1.22	< 7.1	$< 0.7\%$	0.50-0.60 (7.84- 8.87)
4	HMS	11.0	3.50	30.0	0.22	< 1.7	$< 0.1\%$	0.65-0.77 (9.59-10.54)
A	SHMS	11.0	5.80	12.5	465.54	< 0.6	$< 0.1\%$	0.25-0.55 (2.71- 3.77)
B	SHMS	11.0	3.00	30.0	1.54	< 9.5	$< 0.8\%$	0.45-0.77 (7.52-10.54)
C	SHMS	11.0	2.25	30.0	4.69	< 41.9	$< 9.2\%$	0.35-0.55 (5.94- 8.21)

the electron asymmetry. The uncertainty in the pion asymmetry is

$$\Delta A_{\pi^-} = \frac{1}{\sqrt{N_{\pi^-}}} = \frac{1}{\sqrt{\alpha_{\pi/e} N_{e^-}}} = \frac{1}{\sqrt{\alpha_{\pi/e}}} \Delta A_{e^-, DIS, stat.} \quad (15)$$

thus the relative uncertainty in $A_{e^-, DIS}$ after correcting for the pion background is

$$\Delta A_{e^-, DIS, \pi^-} = \frac{\alpha_{\pi/e}}{\eta_{\pi^-, rej}} \Delta A_{\pi^-} = \frac{\sqrt{\alpha_{\pi/e}}}{\eta_{\pi^-, rej}} \Delta A_{e^-, DIS, stat.} \quad (16)$$

which even in the worst case (kinematics #3) is well below 1% of statistical uncertainty and can be safely neglected.

2.6 Pair Production Background

Another background process is the $e - e^+$ pair production. To correct for the dilution and possible asymmetry due to this process, we plan to reverse the spectrometer polarity and measure the asymmetry of scattered positrons. Assuming that the e^+e^- pairs are symmetric and the asymmetry of the e^- is the same as the positron asymmetry, we can correct for this background by subtracting the e^+ asymmetry.

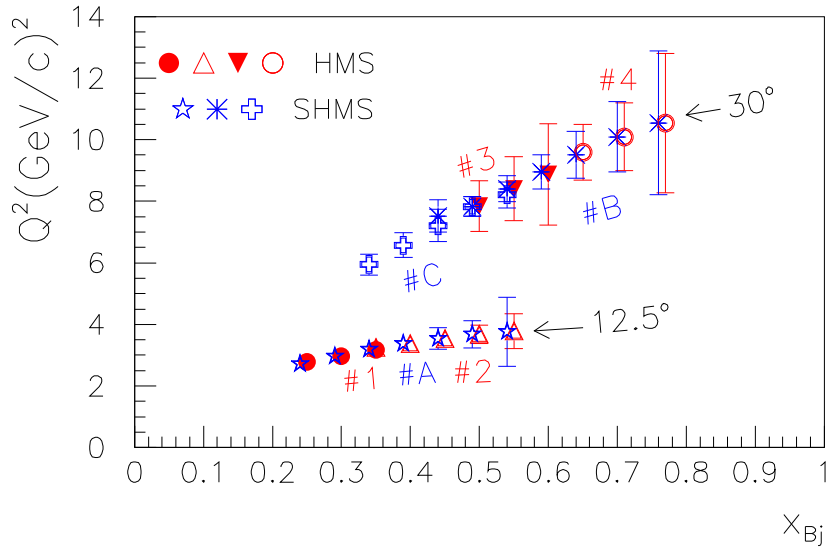
We denote the ratio of e^+ (pair production) to e^- (DIS) rate to be α , then the measured asymmetry is

$$A_{raw} = \frac{A_{e^-, DIS}}{1 + \alpha} + A_{e^+} \frac{\alpha}{1 + \alpha} \quad (17)$$

We correct for A_{e^+} such that $A_{e^-, DIS} = (1 + \alpha)A_{raw} - \alpha A_{e^+}$. Assuming the beam time with zero pair production background is T_0 and the statistical uncertainty we need to

reach is $\Delta A_{e^-,DIS}^{goal}$, now we need βT_0 ($\beta > 1$) to compensate for the dilution factor $(1 + \alpha)$ and γT_0 with reversed polarity to measure A_{e^+} , then the final asymmetry is $A_{e^-,DIS} = \sqrt{\frac{1+\alpha}{\beta} + \frac{\alpha^2}{\gamma}} \Delta A_{e^-,DIS}^{goal}$. Fixing the total beam time $(\beta + \gamma)T_0$ we find $\beta/\gamma = \sqrt{1 + \alpha}/\alpha$ and $A_{e^-,DIS} = \sqrt{\frac{1+\alpha+\alpha\sqrt{1+\alpha}}{\beta}} \Delta A_{e^-,DIS}^{goal}$. Therefore we need to increase the beam time by a factor of $(\alpha + \sqrt{1 + \alpha})^2$, of which $\alpha(\alpha + \sqrt{1 + \alpha})T_0$ will be used for reversed polarity. Or reversely, if the total time is fixed to be T , then $\frac{\alpha}{(\alpha + \sqrt{1 + \alpha})}T$ will be used for reversed polarity running, and the statistical uncertainty on the measured asymmetry is $(\alpha + \sqrt{1 + \alpha})$ times the “ideal” case uncertainty where there is no pair production background and all T is spent on negative polarity running. From Table 2, only 30° settings have non-negligible ($\geq 0.1\%$) pair production background. For kinematics #4 #5 (and #3 for the HMS), the beam time for reversed polarity running will be about 5% of the total beam time at these settings. For the SHMS at kinematics #3, about 20% of beam time will be spent on positive polarity running.

Figure 5: Kinematic coverage of A_1^n measurement using HMS and SHMS with a 11 GeV beam. The higher (lower) Q^2 settings correspond to a scattering angle of 30° (12.5°). And for each angle setting, the solid (open) markers are for the lower (higher) momentum settings. Kinematic points with overlapping x and Q^2 bins are shifted horizontally for clarity. The error bars are proportional to the expected statistical uncertainties on A_1^n . Here we try to match ΔA_1^n (stat.) at the two different Q^2 values. At highest x settings (30° angle), the smaller angle acceptance of the SHMS is compensated by its large y_{targ} acceptance, hence error bars from the SHMS is about the same as those from the HMS. Statistical uncertainties combining the two spectrometers and different kinematics are given in section 4.



2.7 Elastic and $\Delta(1232)$ Asymmetries

In order to check the product of beam and target polarization $P_b P_t$, we plan to measure the longitudinal asymmetry of $e^- - {}^3\vec{\text{He}}$ elastic scattering to 1% (stat.) at a low Q^2 using 2.2 GeV beam. To check the sign of transverse asymmetry, we will measure the asymmetry of $\Delta(1232)$ production with the target spin aligned perpendicular to the beam direction. The kinematic settings for these two measurements are given in Table 3.

Table 3: Kinematics for elastic longitudinal and $\Delta(1232)$ transverse asymmetries. The HMS and SHMS will have the same momentum and angle settings.

Kine	E_b GeV	E_p GeV	θ ($^\circ$)	elastic x-sec (nb/sr)	elastic rate (Hz)	Asymmetry	Time (hours)
Elastic	2.200	2.160	12.5	106.986	710.1	$A_{\parallel} = 0.0589$	7.4
$\Delta(1232)$	2.200	1.815	12.5	-	-	$A_{\perp} \sim \text{a few \%}$	6

3 Data Analysis and Systematic Uncertainties

3.1 Data Analysis Procedure for $A^{3\text{He}}$

The raw asymmetries can be extracted from helicity-dependent yield as

$$A_{raw} = \frac{N^+/(Q^+\eta_{LT}^+) - N^-/(Q^-\eta_{LT}^-)}{N^+/(Q^+\eta_{LT}^+) + N^-/(Q^-\eta_{LT}^-)} \quad (18)$$

where N^h are counts, Q^h are integrated beam charge and η_{LT}^h are live-time of the DAQ. The uncertainties on η_{LT}^h and Q^h are at levels of 0.3% and 0.5%, respectively, and therefore are negligible compared to statistical and other systematic uncertainties.

From measured asymmetries one can extract physics asymmetries as

$$A_{\parallel,\perp} = \frac{A_{raw}}{P_b P_t f_n} \quad (19)$$

where $P_b = 0.85$, $P_t = 0.5$ are beam and target polarizations and can be measured to 1% and 4%, respectively; f_n is the dilution factor due to unpolarized N_2 in the target. For a typical target cell one has $f_n = 0.90 - 0.95$ with an uncertainty of 0.3%.

From measured A_{\parallel} and A_{\perp} one can extract $A_1^{3\text{He}}$ as

$$A_1 = \frac{A_{\parallel}}{D(1 + \eta\xi)} - \frac{A_{\perp}\eta}{d(1 + \eta\xi)} \quad (20)$$

where

$$D = \frac{1 - (1 - y)\epsilon}{1 + \epsilon R}, \quad \text{with } y = \frac{\nu}{E}, \quad \epsilon = \frac{1}{1 + 2(1 + 1/\gamma^2)\tan^2(\theta/2)} \quad (21)$$

$$\eta = \frac{\epsilon\sqrt{Q^2}}{E - E'\epsilon}, \quad \xi = \frac{\eta(1 + \epsilon)}{2\epsilon}, \quad \text{and } d = D\sqrt{\frac{2\epsilon}{1 + \epsilon}} \quad (22)$$

3.2 Nuclear Corrections

Then the neutron asymmetry A_1^n is extracted from $A_1^{3\text{He}}$ as [66]

$$A_1^n = \frac{F_2^{3\text{He}}[A_1^{3\text{He}} - 2\frac{F_2^p}{F_2^{3\text{He}}}P_p A_1^p(1 - \frac{0.014}{2P_p})]}{P_n F_2^n(1 + \frac{0.056}{P_n})}, \quad (23)$$

where $P_n = 0.86_{-0.02}^{+0.036}$ and $P_p = -0.028_{-0.004}^{+0.009}$ are effective nucleon polarizations of the neutron and the proton inside ^3He and their current known value and full uncertainties evaluated from three N-N potential calculations [67, 66, 68]. The uncertainty on P_p dominated the systematic uncertainty for the previous A_1^n measurement. The approved Hall A experiment E05-102 [69] is aiming in studying the ^3He wavefunction and the uncertainties on P_n and P_p will be improved by a factor of 4 after the completion of this experiment. We therefore take $\Delta P_p = 0.003$ in our uncertainty analysis. We used a fit to world g_1^p/F_1^p data [41] to estimate the uncertainty on A_1^p needed in Eq. (23).

For the unpolarized structure functions F_2 in Eq. (23), we use the latest unpolarized PDF parameterizations [70, 71] to construct F_1 and a parameterization for R [72]. The uncertainties in F_2 are evaluated using the uncertainties of PDF's, R 's, as well as the difference between the two PDF parameterizations.

3.3 Systematic Uncertainties

The systematic uncertainty on A_1^n is dominated by the following terms:

1. Effective proton polarization in the ^3He : $P_p = -0.028 \pm 0.003$
2. Unpolarized structure functions F_1 : constructed from PDF parameterizations. We used the weighted average of MRST and CTEQ for the uncertainty on F_1^p and F_1^n ³.
3. Proton spin asymmetry A_1^p : from a fit to world g_1^p/F_1^p data, with uncertainties [41];
4. Beam and target polarizations $P_b = 0.85(1 \pm 1\%)$ and $P_t = 0.50(1 \pm 3\%)$.

Figure 7 in the next section illustrate the above contributions to the systematic uncertainties of A_1^n at all x .

³However, there is uncertainty in F_1^n due to nuclear effects in the deuteron, which is not included in either MRST or CTEQ analysis. This uncertainty will shift the A_1^n value for all x and hence is an correlated uncertainty.

4 Expected Results and Complementarity to the Hall A BigBite Proposal

4.1 Expected Results for A_1^n and Uncertainties

Projected results for A_1^n and their uncertainties are shown in Fig. 6. For rate estimation we compare the cross section calculated from the NMC F_2 , and the CTEQ and the MRST parameterizations. We found that both CTEQ and MRST give slightly higher cross sections than NMC in the region $x < 0.4$, but much lower ones for large x , varying from 30% lower at $x = 0.6$ to 60% lower at $x = 0.77$. To be on the safe side, we take the smallest cross section among three parameterizations at all x . We use 80% and 50% for beam and target polarizations, respectively. The target length is 40 cm and the maximum beam current is 15 μA . The error bars show the expected statistical error and the error bands around the horizontal axis illustrate the expected systematic uncertainties. It is dominated by beam and target polarimetry and the error in ^3He nuclear corrections, which is further determined by the knowledge of the proton spin asymmetry A_1^p . Here we estimate the uncertainty in A_1^p assuming a similar amount of beam time as proposed here will be used to measure A_1^p using a NH_3 target. In Fig. 6, the horizontal axis shows the

Table 4: Projected statistical and systematic uncertainties at different x and Q^2 .

x	$\Delta A_1^n(\text{stat.})$ low Q^2	$\Delta A_1^n(\text{stat.})$ high Q^2	$\Delta A_1^n(\text{stat.})$ two Q^2 combined	$\Delta A_1^n(\text{syst.})$	$\Delta A_1^n(\text{total})$
0.25	0.0037	—	0.0037	0.0050	0.0062
0.30	0.0043	—	0.0043	0.0060	0.0074
0.35	0.0052	0.0180	0.0050	0.0072	0.0088
0.40	0.0061	0.0212	0.0059	0.0087	0.0104
0.45	0.0082	0.0259	0.0078	0.0103	0.0129
0.50	0.0111	0.0124	0.0083	0.0123	0.0148
0.55	—	0.0170	0.0136	0.0147	0.0200
0.60	—	0.0239	0.0239	0.0176	0.0297
0.65	—	0.0254	0.0254	0.0211	0.0330
0.71	—	0.0343	0.0343	0.0260	0.0430
0.77	—	0.0706	0.0706	0.0317	0.0774

SU(6) prediction that $A_1^n = 0$. The curves illustrate (from top to bottom in the region $x > 0.6$): 1) the LSS(BBS) parameterization at $Q^2 = 4 \text{ (GeV/c)}^2$ (short-dashed, light blue) [35]; 2) the BBS parameterization at $Q^2 = 4 \text{ (GeV/c)}^2$ (long-dashed, blue) [34]; 3) the chiral soliton prediction by Weigel et al. [49, 50, 51] (long-dashed, magenta); 4) the RCQM [32] (yellow shaded band); 5) the LSS2001 parameterization (solid, black) [47, 73]; and 6) another chiral soliton prediction by Wakamatsu (short-dashed, magenta) [52, 53].

Data shown are from SLAC E142 [74] and E154 [75, 76], HERMES [77], and JLab 6 GeV E99-117 [40].

Figure 6: Projected data (red solid circles) for measurements of asymmetries A_1^n in the large- x DIS region using a 11 GeV beam and HMS and SHMS in Hall C. See text for explanation of expected uncertainties, theoretical predictions and existing data.

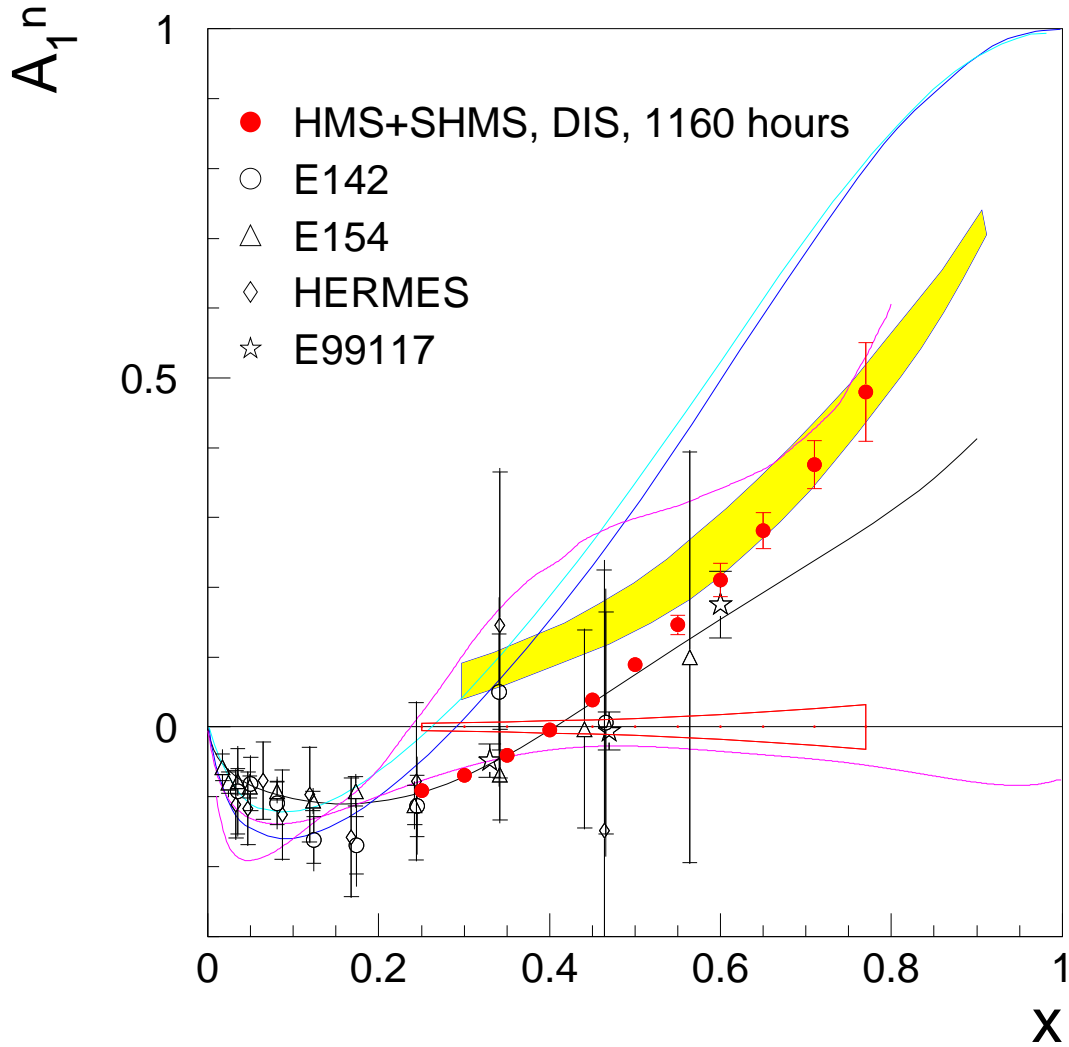


Figure 7: Statistical and systematic uncertainties for the proposed A_1^n measurement.

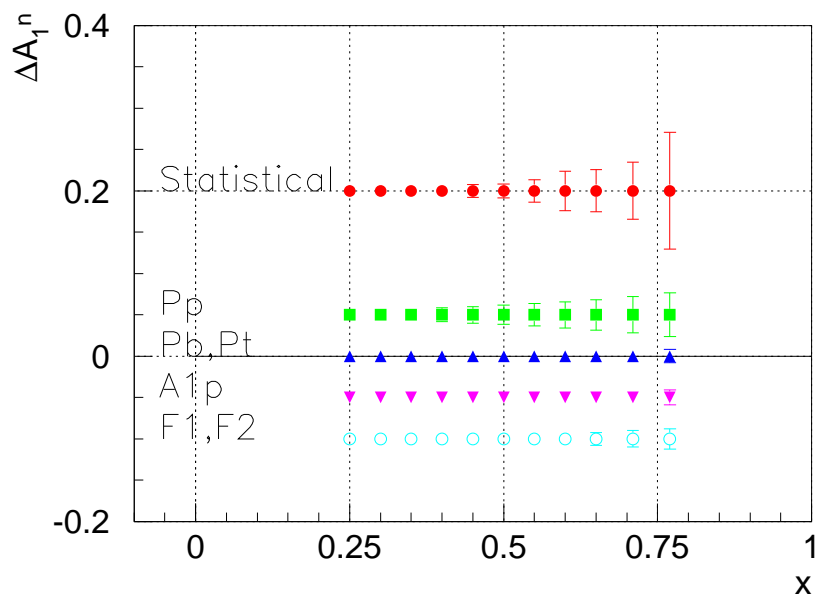
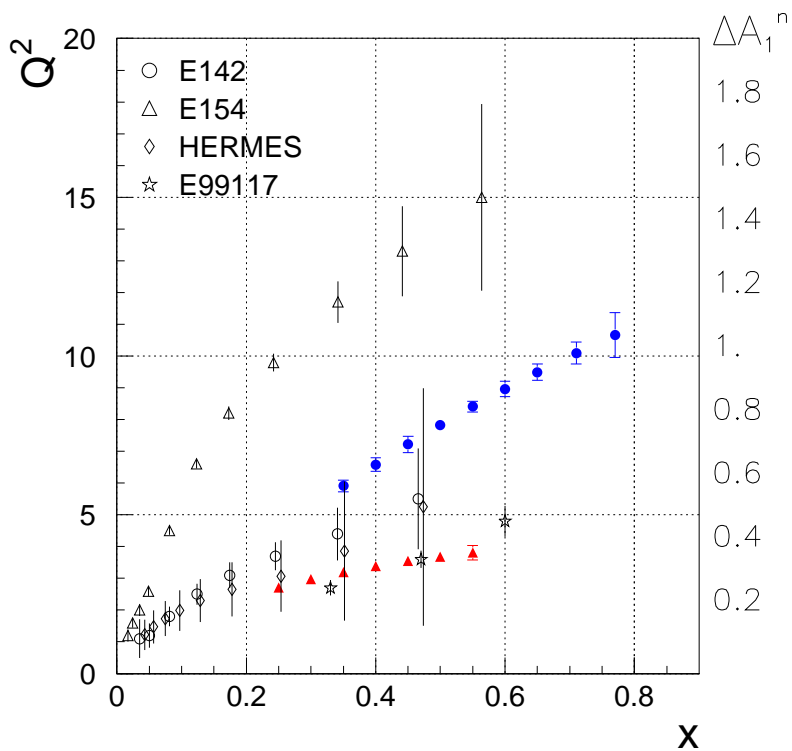


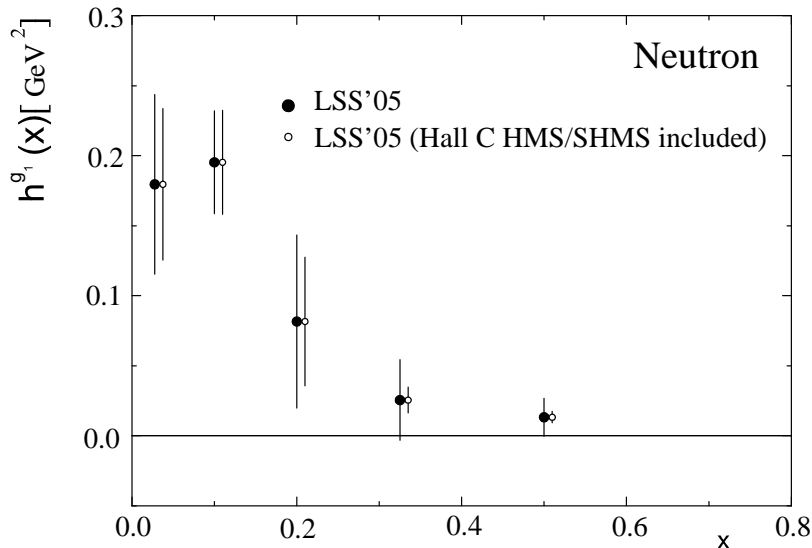
Figure 8: Statistical uncertainty of A_1^n from HMS+SHMS at 30° (blue solid circles) and 12.5° (red solid triangles) plotted on a x - Q^2 plane. The scale of the error bars are given on the vertical axis on the right. Statistical uncertainties of previous world data (open markers) are also shown for comparison.



4.2 Expected Results for Neutron $h^{g_1}(x)$

From Eq. (14) one can extract the higher-twist contribution to $g_1^n(x, Q^2)$. Results from a global analysis with the new data included are shown in Fig. 9.

Figure 9: Expected uncertainties for the higher-twist contribution to $g_1^n(x, Q^2)$ extracted from a global analysis. Current knowledge on this function is shown by solid circle and the projected results are shown as the open circles.

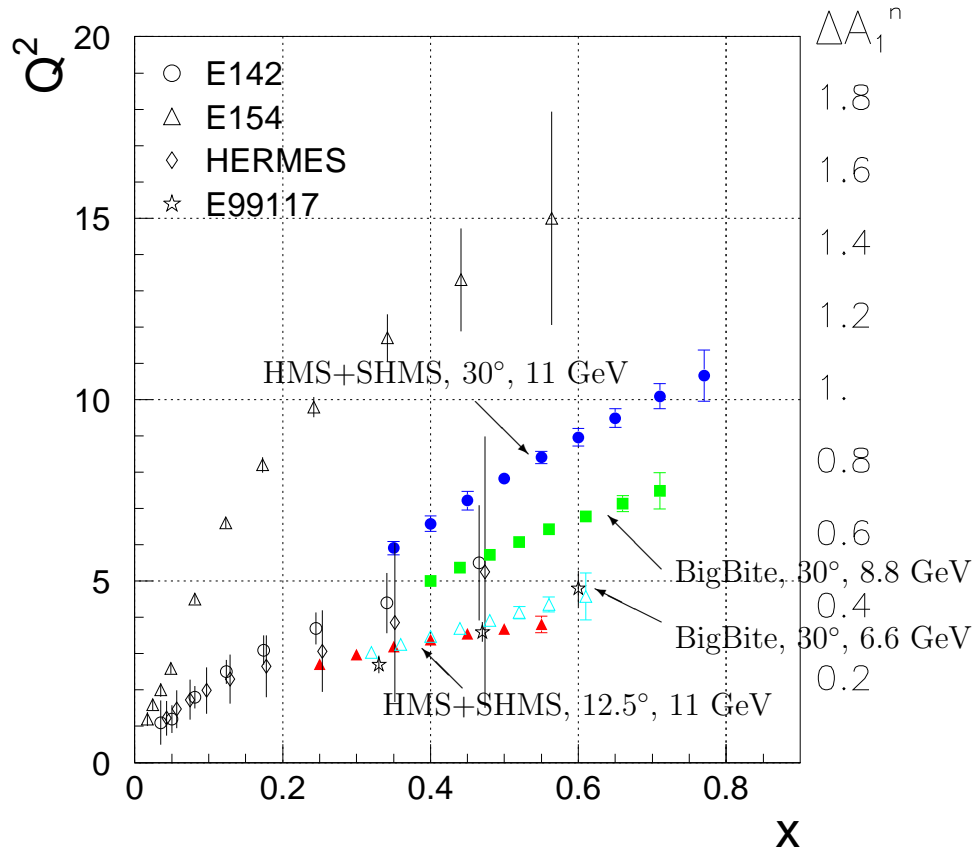


4.3 Complementarity to the Hall A proposal

A measurement of A_1^n using an 8.8 GeV beam and the BigBite spectrometer in Hall A [78] is being proposed at the same time as the measurement described in this document. The major difference between these two proposals, at the first sight, is in the experimental setup. The large solid angle and momentum acceptances of the BigBite spectrometer help to obtain similar statistics within a short amount of beam time. However the open geometry of BigBite makes it more difficult and challenging for carrying out inclusive measurement than HMS and SHMS.

The more important difference is in their kinematic coverage, see Fig. 10. The measurements proposed here will cover Q^2 values both higher and lower than the BigBite proposal to a high precision. On the other hand, projected results from the BigBite proposal, if combined with the proposed measurement in Hall C, will cover a more complete Q^2 range and will provide better understanding of the Q^2 -evolution of A_1^n , of which the physics importance was discussed in Section 1.4.

Figure 10: Complimentary of this proposal and the BigBite proposal in Hall A. Statistical uncertainty of A_1^n expected from this proposal (blue solid circles and red solid triangles) and from the BigBite proposal (green solid squares and cyan open triangles) are plotted on a $x-Q^2$ plane. The scale of the error bars are given on the vertical axis on the right. Previous world data (open markers) are also shown for comparison.



5 Beam Time Request and Contributions to Hall C 12 GeV Equipment

5.1 Beam Time Request

The beam time allocation for production runs at each kinematics is shown in Table 5.

Table 5: Beam time (total 1162 hours) for DIS measurements.

Kine	E_b (GeV)		θ ($^\circ$)	E_p (GeV)	e^- production (hours)	e^+ prod. (hours)	Tot. Time (hours)
1	11.0	HMS	12.5	5.70	24	0	24
2	11.0	HMS	12.5	6.80	48	0	48
3	11.0	HMS	30.0	2.82	109	1	110
4	11.0	HMS	30.0	3.50	979	1	980
A	11.0	SHMS	12.5	5.80	72	0	72
B	11.0	SHMS	30.0	3.00	903	7	910
C	11.0	SHMS	30.0	2.25	165	15	180
1	11.0	HMS	12.5	5.70	24	0	24
2	11.0	HMS	12.5	6.80	48	0	48
3	11.0	HMS	30.0	2.82	110	0	110
4	11.0	HMS	30.0	3.50	980	0	980
A	11.0	SHMS	12.5	5.80	72	0	72
B	11.0	SHMS	30.0	3.00	910	0	910
C	11.0	SHMS	30.0	2.25	180	0	180

Additional beam time include:

- To check the dilution factor due to unpolarized material in the target, we need to measure the nitrogen cross section using reference cells: 2 hours at kinematics 1 (A), 2 (A), and 4 hours at kinematics B, 3 (C) and 4 (C). This requires a total of 16 hours for DIS production settings;
- To check the product of beam and target polarizations $P_b P_t$ and to check the sign of transverse asymmetries, we need 16 hours to measure the longitudinal asymmetry of $\vec{e}^- - {}^3\vec{\text{He}}$ elastic scattering (including N_2 reference cell runs) and 6 hours to measure the transverse asymmetry of $\Delta(1232)$ production. The beam energy for these two measurements will be 2.2 GeV and both SHMS and HMS will be set at 12.5° ;
- beam pass change from 2.2 to 11 GeV, 8 hours;

- beam polarization measurements: non-invasive for Compton and 8 hours for 2 Moller measurements (one at each beam energy);
- configuration changes: 10 (angle or momentum) \times 0.5 hours + 8 (polarity) = 13 hours;
- target polarization measurements, about 3% of production time (that’s 40 minutes per day), or 32 hours.

The total beam time request is 1261 hours, or 52.6 days.

5.2 Contributions to Hall C 12 GeV Equipment

The polarized ^3He collaboration will install the polarized ^3He target in Hall C. In addition, the University of Virginia and the Temple University groups are committed to make at least 2 FTE-years contribution to Hall C beamline commissioning at the 12 GeV Upgrade, including the Compton and the Moller polarimetry, the ARC energy measurement and the raster system.

6 Summary

We request for 1261 hours of beam time to measure neutron spin asymmetry A_1^n in the deep inelastic scattering region $0.3 < x < 0.77$ and $3 < Q^2 < 10$ (GeV/c) 2 . The proposed measurement will extend our present knowledge of A_1^n from $x = 0.60$ to $x = 0.77$ and its wide Q^2 coverage will explore possible Q^2 -dependence of A_1^n . If combined with the proposed Hall A A_1^n measurement using the BigBite spectrometer, the Q^2 -dependence of A_1^n will be studied to a greater accuracy. Results from this measurement will provide the first precise data in the unexplored “deep” valence quark region and therefore test various predictions including those from the relativistic constituent quark model and perturbative QCD.

References

- [1] J. Ashman et al. A measurement of the spin asymmetry and determination of the structure function $g(1)$ in deep inelastic muon proton scattering. *Phys. Lett.*, B206:364, 1988.
- [2] J. Ashman et al. An investigation of the spin structure of the proton in deep inelastic scattering of polarized muons on polarized protons. *Nucl. Phys.*, B328:1, 1989.
- [3] M. J. Alguard et al. Deep inelastic e p asymmetry measurements and comparison with the bjorken sum rule and models of the proton spin structure. *Phys. Rev. Lett.*, 41:70, 1978.

- [4] Guenter Baum et al. A new measurement of deep inelastic e p asymmetries. *Phys. Rev. Lett.*, 51:1135, 1983.
- [5] F. E. Close. On the transformation between current and constituent quarks and consequences for polarized electroproduction structure functions. *Nucl. Phys.*, B80:269, 1974.
- [6] A. Le Yaouanc, L. Oliver, O. Pene, and J. C. Raynal. Prediction of the $su(3) \times su(3)$ configuration mixing as a relativistic effect in the naive quark model. *Phys. Rev.*, D9:2636, 1974.
- [7] A. Le Yaouanc, L. Oliver, O. Pene, and J. C. Raynal. Combined effects of internal quark motion and $su(6)$ breaking on the properties of the baryon ground state. *Phys. Rev.*, D15:844, 1977.
- [8] A. Chodos, R. L. Jaffe, K. Johnson, and Charles B. Thorn. Baryon structure in the bag theory. *Phys. Rev.*, D10:2599, 1974.
- [9] Michael J. Ruiz. Covariant harmonic oscillators and the axial - vector coupling constant. *Phys. Rev.*, D12:2922, 1975.
- [10] Cameron Hayne and Nathan Isgur. Beyond the wave function at the origin: Some momentum dependent effects in the nonrelativistic quark model. *Phys. Rev.*, D25:1944, 1982.
- [11] Z. Dziembowski, C. J. Martoff, and P. Zyla. Deep inelastic spin and flavor asymmetry of the nucleon from a qcd inspired quark model. *Phys. Rev.*, D50:5613–5626, 1994.
- [12] Bo-Qiang Ma. The x-dependent helicity distributions for valence quarks in nucleons. *Phys. Lett.*, B375:320–326, 1996.
- [13] B. W. Filippone and Xiang-Dong Ji. The spin structure of the nucleon. *Adv. Nucl. Phys.*, 26:1, 2001.
- [14] Xiang-Dong Ji. Gauge invariant decomposition of nucleon spin. *Phys. Rev. Lett.*, 78:610–613, 1997.
- [15] R. L. Jaffe and Aneesh Manohar. The $g(1)$ problem: Fact and fantasy on the spin of the proton. *Nucl. Phys.*, B337:509–546, 1990.
- [16] G. Morpurgo. Is a nonrelativistic approximation possible for the internal dynamics of elementary particles? *Physics (N.Y.)*, 2(2):95, 1965.
- [17] R.H. Dalitz. High energy physics lectures delivered during the 1965 session of the summer school of theoretical physics, university of grenoble, 1965.

- [18] A. Bodek et al. Comparisons of deep inelastic e p and e n cross-sections. *Phys. Rev. Lett.*, 30:1087, 1973.
- [19] E. M. Riordan et al. Extraction of $r = \sigma_l / \sigma_t$ from deep inelastic e p and e d cross-sections. *Phys. Rev. Lett.*, 33:561, 1974.
- [20] J. S. Poucher et al. High-energy single arm inelastic e - p and e - d scattering at 6-degrees and 10-degrees. *Phys. Rev. Lett.*, 32:118, 1974.
- [21] A. C. Benvenuti et al. A comparison of the structure functions f_2 of the proton and the neutron from deep inelastic muon scattering at high q^2 . *Phys. Lett.*, B237:599, 1990.
- [22] J. J. Aubert et al. Measurements of the nucleon structure functions f_2 (n) in deep inelastic muon scattering from deuterium and comparison with those from hydrogen and iron. *Nucl. Phys.*, B293:740, 1987.
- [23] D. Allasia et al. Measurement of the neutron and the proton f_2 structure function ratio. *Phys. Lett.*, B249:366–372, 1990.
- [24] P. Amaudruz et al. The gottfried sum from the ratio $f_2(n) / f_2(p)$. *Phys. Rev. Lett.*, 66:2712–2715, 1991.
- [25] P. Amaudruz et al. The ratio $f_2(n) / f_2(p)$ in deep inelastic muon scattering. *Nucl. Phys.*, B371:3–31, 1992.
- [26] M. R. Adams et al. Extraction of the ratio f_2^n / f_2^p from muon - deuteron and muon - proton scattering at small x and q^2 . *Phys. Rev. Lett.*, 75:1466–1470, 1995.
- [27] K. Abe et al. Measurements of the proton and deuteron spin structure functions g_1 and g_2 . *Phys. Rev.*, D58:112003, 1998.
- [28] B. Adeva et al. Spin asymmetries a_1 of the proton and the deuteron in the low x and low q^2 region from polarized high energy muon scattering. *Phys. Rev.*, D60:072004, 1999.
- [29] F. E. Close. $Nu w(2)$ at small ω' and resonance form-factors in a quark model with broken $su(6)$. *Phys. Lett.*, B43:422–426, 1973.
- [30] Robert D. Carlitz. $Su(6)$ symmetry breaking effects in deep inelastic scattering. *Phys. Lett.*, B58:345, 1975.
- [31] A. De Rujula, Howard Georgi, and S. L. Glashow. Hadron masses in a gauge theory. *Phys. Rev.*, D12:147–162, 1975.
- [32] Nathan Isgur. Valence quark spin distribution functions. *Phys. Rev.*, D59:034013, 1999.

- [33] Glennys R. Farrar and Darrell R. Jackson. Pion and nucleon structure functions near $x = 1$. *Phys. Rev. Lett.*, 35:1416, 1975.
- [34] Stanley J. Brodsky, Matthias Burkardt, and Ivan Schmidt. Perturbative qcd constraints on the shape of polarized quark and gluon distributions. *Nucl. Phys.*, B441:197–214, 1995.
- [35] Elliot Leader, Aleksander V. Sidorov, and Dimiter B. Stamenov. Nlo qcd analysis of polarized deep inelastic scattering. *Int. J. Mod. Phys.*, A13:5573–5592, 1998.
- [36] D. Abbott et al. Measurement of tensor polarization elastic electron deuteron scattering at large momentum transfer. *Phys. Rev. Lett.*, 84:5053–5057, 2000.
- [37] K. Wijesooriya et al. Polarization measurements in neutral pion photoproduction. *Phys. Rev.*, C66:034614, 2002.
- [38] M. K. Jones et al. $G(e(p))/g(m(p))$ ratio by polarization transfer in $e(\text{pol.}) p \rightarrow e p(\text{pol.})$. *Phys. Rev. Lett.*, 84:1398–1402, 2000.
- [39] O. Gayou et al. Measurement of g_e^p/g_m^p in $e\vec{p} \rightarrow e\vec{p}$ to $q^2 = 5.6 \text{ geV}^2$. *Phys. Rev. Lett.*, 88:092301, 2002.
- [40] X. Zheng et al. Precision measurement of the neutron spin asymmetry $a(1)(n)$ and spin-flavor decomposition in the valence quark region. *Phys. Rev. Lett.*, 92:012004, 2004.
- [41] X. Zheng et al. Precision measurement of the neutron spin asymmetries and spin-dependent structure functions in the valence quark region. *Phys. Rev.*, C70:065207, 2004.
- [42] G. Peter Lepage and Stanley J. Brodsky. Exclusive processes in perturbative quantum chromodynamics. *Phys. Rev.*, D22:2157, 1980.
- [43] Gerald A. Miller and Michael R. Frank. Q^{*2} independence of $qf(2)/f(1)$, poincare invariance and the non-conservation of helicity. *Phys. Rev.*, C65:065205, 2002.
- [44] John P. Ralston, Pankaj Jain, and Roman V. Buniy. The transverse quark distribution and proton electromagnetic form factors in skew distribution formalism. *AIP Conf. Proc.*, 549:302, 2000.
- [45] Andrei V. Belitsky, Xiang-dong Ji, and Feng Yuan. A perturbative qcd analysis of the nucleon's pauli form factor $f_2(q^{*2})$. *Phys. Rev. Lett.*, 91:092003, 2003.
- [46] Xiang-dong Ji, Jian-Ping Ma, and Feng Yuan. Three-quark light-cone amplitudes of the proton and quark- orbital-motion dependent observables. *Nucl. Phys.*, B652:383–404, 2003.

- [47] Elliot Leader, Aleksander V. Sidorov, and Dimiter B. Stamenov. A new evaluation of polarized parton densities in the nucleon. *Eur. Phys. J.*, C23:479–485, 2002.
- [48] Claude Bourrely, Jaques Soffer, and Franco Buccella. A statistical approach for polarized parton distributions. *Eur. Phys. J.*, C23:487–501, 2002.
- [49] H. Weigel, L. P. Gamberg, and H. Reinhardt. Nucleon structure functions from a chiral soliton. *Phys. Lett.*, B399:287–296, 1997.
- [50] H. Weigel, L. P. Gamberg, and H. Reinhardt. Polarized nucleon structure functions within a chiral soliton model. *Phys. Rev.*, D55:6910–6923, 1997.
- [51] O. Schroeder, H. Reinhardt, and H. Weigel. Nucleon structure functions in the three flavor njl soliton model. *Nucl. Phys.*, A651:174, 1999.
- [52] M. Wakamatsu. Light-flavor sea-quark distributions in the nucleon in the su(3) chiral quark soliton model. i. phenomenological predictions. *Phys. Rev.*, D67:034005, 2003.
- [53] Masashi Wakamatsu. Light-flavor sea-quark distributions in the nucleon in the su(3) chiral quark soliton model. ii: Theoretical formalism. *Phys. Rev.*, D67:034006, 2003.
- [54] C. Boros and Anthony W. Thomas. Parton distributions for the octet and decuplet baryons. *Phys. Rev.*, D60:074017, 1999.
- [55] F.M. Steffens and A.W. Thomas. priv. comm.
- [56] Elliott D. Bloom and Frederick J. Gilman. Scaling, duality, and the behavior of resonances in inelastic electron - proton scattering. *Phys. Rev. Lett.*, 25:1140, 1970.
- [57] Elliott D. Bloom and Frederick J. Gilman. Scaling and the behavior of nucleon resonances in inelastic electron - nucleon scattering. *Phys. Rev.*, D4:2901, 1971.
- [58] F. E. Close and W. Melnitchouk. Symmetry breaking and quark hadron duality in structure functions. *Phys. Rev.*, C68:035210, 2003.
- [59] M. Anselmino, A. Efremov, and E. Leader. The theory and phenomenology of polarized deep inelastic scattering. *Phys. Rept.*, 261:1–124, 1995.
- [60] Elliot Leader, Aleksander V. Sidorov, and Dimiter B. Stamenov. Longitudinal polarized parton densities updated. *Phys. Rev.*, D73:034023, 2006.
- [61] R. Ent. Jlab hall c 12 gev upgrade meeting presentations, url: http://www.jlab.org/hall-c/upgrade/12gev_mtg_051106.pdf.
- [62] J. Alcorn et al. Basic instrumentation for hall a at jefferson lab. *Nucl. Instrum. Meth.*, A522:294–346, 2004.

- [63] G.D. Cates, K. McCormick, B. Reitz, and B Wojtsekhowski. Measurement of the neutron electric form factor g_e^n at high q^2 .
- [64] E. Babcock, I. Nelson, S. Kadlecik, B. Driehuys, L.D. Anderson, F.W. Hersman, and Walker T.G. Hybrid spin-exchange optical pumping of ^3he . *Phys. Rev. Lett.*, 91:123003, 2003.
- [65] David E. Wiser. *INCLUSIVE PHOTOPRODUCTION OF PROTONS, KAONS, AND PIONS AT SLAC ENERGIES*. PhD thesis, Univ. of Wisconsin, 1977. UMI 77-19743.
- [66] F. Bissey, V. Guzey, M. Strikman, and Anthony W. Thomas. Complete analysis of spin structure function g_1 of he-3. *Phys. Rev.*, C65:064317, 2002.
- [67] Claudio Ciofi degli Atti, S. Scopetta, E. Pace, and G. Salme. Nuclear effects in deep inelastic scattering of polarized electrons off polarized he-3 and the neutron spin structure functions. *Phys. Rev.*, C48:968–972, 1993.
- [68] A. Nogga. *Nuclear and Hypernuclear Three- and Four-Body Bound States*. PhD thesis, Ruhr-Universitat Bochum, 2001.
- [69] S. Gilad, D. Higinbotham, W. Korsch, B. Norum, and S. Sirca. Measurements of a_x and a_z asymmetries in the quasi-elastic $^3\text{he}(e,e'd)$ reaction.
- [70] J. Pumplin et al. New generation of parton distributions with uncertainties from global qcd analysis. *JHEP*, 07:012, 2002.
- [71] Alan D. Martin, R. G. Roberts, W. J. Stirling, and R. S. Thorne. Mrst2001: Partons and alpha(s) from precise deep inelastic scattering and tevatron jet data. *Eur. Phys. J.*, C23:73–87, 2002.
- [72] K. Abe et al. Measurements of $r = \sigma_l/\sigma_t$ for $0.03 < x < 0.1$ and fit to world data. *Phys. Lett.*, B452:194–200, 1999.
- [73] D.B. Stamenov E. Leader. priv. comm.
- [74] P. L. Anthony et al. Deep inelastic scattering of polarized electrons by polarized he-3 and the study of the neutron spin structure. *Phys. Rev.*, D54:6620–6650, 1996.
- [75] K. Abe et al. Precision determination of the neutron spin structure function g_1^n . *Phys. Rev. Lett.*, 79:26–30, 1997.
- [76] K. Abe et al. Next-to-leading order qcd analysis of polarized deep inelastic scattering data. *Phys. Lett.*, B405:180–190, 1997.
- [77] K. Ackerstaff et al. Measurement of the neutron spin structure function g_1^n with a polarized he-3 internal target. *Phys. Lett.*, B404:383–389, 1997.

- [78] G.D. Cates, Z.-E. Meziani, N. Liyange, G. Rosner, B. Wojtsekhowski, and X. Zheng. Measurement of a_1^n using the bigbite spectrometer and the 8.8 and the 6.6 gev beam in hall a, July 2006.